JOURNAL OF GEOPHYSICAL RESEARCH, VOL. 114, B06403, doi:10.1029/2008JB006240, 2009

Constraints on continued episodic inflation at Long Valley Caldera, based on seismic and geodetic observations

Lujia Feng[1] and Andrew V. Newman[1]

Received 5 December 2008; revised 6 February 2009; accepted 14 April 2009; published 19 June 2009.

[1] Long Valley Caldera, a large and potentially explosive silicic system, has experienced highly anomalous continued inflation since late 1970s. We characterize an episode of rapid episodic uplift occurring between 2002 and 2003 following similar episodes of 1979–1980, 1983, 1989–1990, and 1997–1998. This most recent episode was the first to be observed by a dense array of 13 continuous Global Positioning System (GPS) stations. Similar to previously observed episodes of deformation, uplift is quasi-radially symmetric and is mostly explained by a compact pressure source located ~3 km west of the resurgent dome. The maximum uplift during the 2002–2003 episode is ~35 ± 8 mm, about 1/3 the magnitude but with a similar time-dependent behavior as the 1997–1998 episode. The horizontal source location is well constrained at −118.930°, 37.678°, for a small spherical source, and indistinguishable from the location of a vertically dipping prolate spheroidal source. A trade-off between depth and volume change is observed for both spherical and prolate models, with depth between 7.5 and 13.5 km and a volume change of 0.01–0.03 km^3 at 95% confidence. For prolate spheroidal models, depth and volume change are additionally affected by the source axis ratio (b/a), which is greater than 0.55. Though the background seismicity remained low during the 2002–2003 episode, we identified a significant spike in activity during the maximum rate of uplift, similar to observations in both the much larger episodes in 1989–1990, and 1997–1998. More interestingly, we additionally find that all three episodes begin immediately after a short period of seismic quiescence, with background seismicity falling to levels below background levels following the prior uplift event. With the dense GPS coverage, we also identify increased opening of the Mono-Inyo volcanic chain after the 2002–2003 episode suggesting potential interaction of magmatic fluids between the two systems.

Citation: Feng, L., and A. V. Newman (2009), Constraints on continued episodic inflation at Long Valley Caldera, based on seismic and geodetic observations, *J. Geophys. Res.*, *114*, B06403, doi:10.1029/2008JB006240.

1. Introduction

[2] Long Valley Caldera (LVC), a 15 × 30 km^2 oval-shaped collapse crater in eastern California (Figure 1), is a volcanic system that was active from ~4 Ma until the last eruptions ~0.1 Ma (see *Bailey et al.* [1976], *Bailey* [1989], *Hildreth* [2004], and *Hill* [2006] for more about the volcanic history). The historic record, however, shows no observable deformation or significant earthquake activity between 1905 and the onset of the current state of unrest beginning in the late 1970s [*Hill*, 2006; *Castle et al.*, 1984].

[3] The recent unrest at LVC is characterized primarily by the uplift of the resurgent dome and recurring earthquake swarms beginning with an $M_L = 5.8$ earthquake on 4 October 1978 [*Savage et al.*, 1981; *Ryall and Ryall*, 1983; *Hill*, 2006]. Synchronous with the onset of seismicity, was the initiation of ongoing episodic uplift. Over the past 30 years, LVC has accumulated ~80 cm of the uplift centered on the resurgent dome (Figure 1) and produced multiple sequences of earthquake swarms in the south moat (Figure 1). The tools to measure the ongoing deformation have changed with time, going from initial leveling and regional triangulation [e.g., *Savage and Clark*, 1982; *Castle et al.*, 1984] to local electronic distance measurements (EDM) [*Langbein*, 1989, 2003; *Langbein et al.*, 1993, 1995] and to campaign and continuous Global Positioning System (GPS) measurements [*Webb et al.*, 1995; *Marshall et al.*, 1997; *Dixon et al.*, 1997; *Newman et al.*, 2006], and interferometric synthetic aperture radar (InSAR) imaging [*Fialko et al.*, 2001; *Newman et al.*, 2006; *Tizzani et al.*, 2007]. With these tools the character of uplift has been identified to consist of periods of episodic accelerated uplift, periods of steady slow inflation, and short-term small-amplitude deflations. The cause of LVC's recently renewed activity remains unclear; however, the location of LVC along a left step in the dextral Eastern California Shear Zone (ECSZ) likely plays an important role in maintaining pathways for magmatic activity [*Hill*, 2006]. Because both the nature of seismicity and deformation reveal details about the ongoing subsurface processes, we briefly review

[1]School of Earth and Atmospheric Sciences, Georgia Institute of Technology, Atlanta, Georgia, USA.

0148-0227/09/2008JB006240$09.00

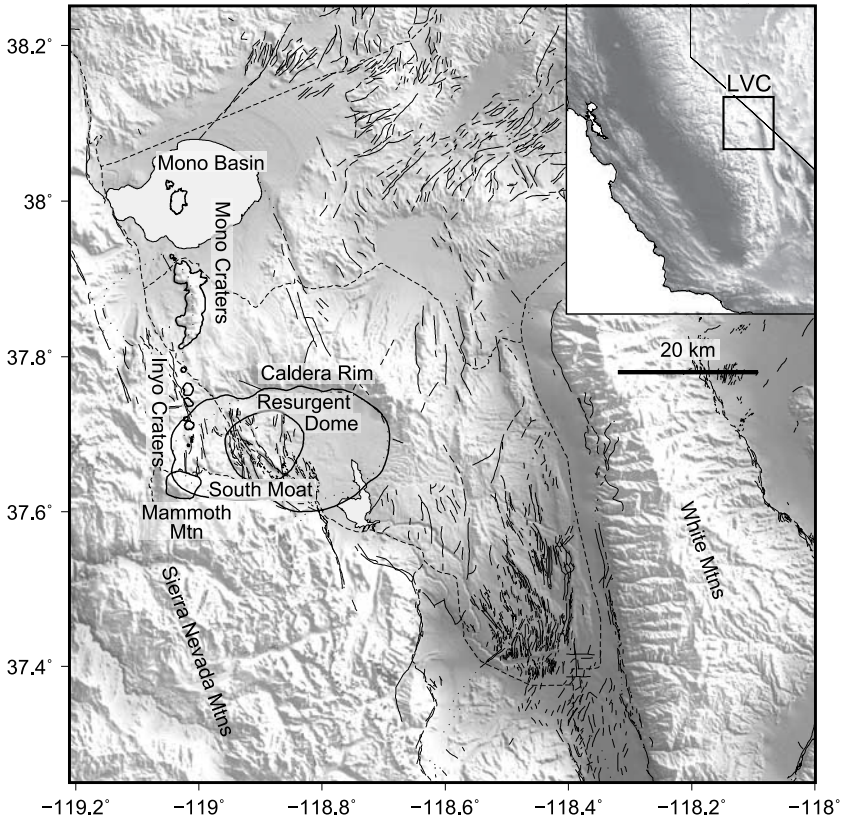

Figure 1. Shaded relief map of Long Valley Caldera and Mono-Inyo volcanic chain. Thick lines outline the caldera topographic rim, the resurgent dome, the Mono-Inyo craters, and Mammoth Mountain. Thin lines show the major faults in and around the Long Valley area. Dashed lines are roads. Inset shows the location of Long Valley Caldera in central eastern California.

the history of both through five episodes of accelerated dome growth (1979–1980, 1983, 1989–1990, 1997–1998 and 2002–2003). The most recent, and previously undocumented, 2002–2003 episode occurred with a level of GPS coverage not available in previous episodes, illuminating interactions between the resurgent dome and the Mono-Inyo volcanic chain (Figure 1) outside of the caldera. This episode is the focus of this paper.

[4] Leveling, which was the major contributor to the early observation, revealed a rapid uplift of at least 25 cm at the resurgent dome in 1979–1980 [*Savage et al.*, 1981; *Savage and Clark*, 1982; *Castle et al.*, 1984]. During this episode, four $M_L \geq 6$ earthquakes on 25–27 May 1980 led the most intensive and vigorous earthquake sequence so far in LVC [*Ryall and Ryall*, 1983; *Denlinger and Riley*, 1984; *Hill*, 2006]. In 1980–1982, LVC continued a steady inflation with additional 10 cm uplift [*Castle et al.*, 1984]. On 7 January 1983, a large earthquake swarm including two M_L = 5.3 events marked the second episode of uplift acceleration [*Savage and Cockerham*, 1984; *Langbein*, 2003; *Hill*, 2006]. The uplift of the resurgent dome increased to ~40 cm by August 1983 [*Castle et al.*, 1984].

[5] Two-color EDM measurements began in 1983 and repeated daily to subannually across the resurgent dome, and other regions in and around the caldera [*Langbein*, 1989]. EDM results documented a long-term slowing inflation with a gradual decrease in the displacement rates from 20 mm/a in 1984 to near zero in mid-1989 across the resurgent dome, as measured between stations CASA and KRAK (Figure 2) [*Langbein*, 1989; *Langbein et al.*, 1993]. The corresponding seismic activity also declined to a relatively low level through this period [*Langbein et al.*, 1993; *Hill*, 2006]. A short period of slight deflation through mid-1989 was recorded by EDM, which coincided with an 11-month-long swarm of small earthquakes under Mammoth Mountain (Figure 1) on the southwest rim of the caldera [*Langbein et al.*, 1993; *Hill*, 2006].

[6] The third episode (1989–1990) started with a dramatic increase of displacement rate to 70 mm/a in late 1989 throughout the first quarter of 1990, which was followed by a markedly increased seismicity two months later in early January 1991 [*Langbein et al.*, 1993]. The rate decreased to 30 mm/a in April 1990 and was fairly steady at this rate through 1995, before slowing down through 1996 and dropping to less than 10 mm/a by the end of April 1997 [*Langbein et al.*, 1993; *Langbein*, 2003; *Hill*, 2006]. Earthquake swarms still resumed in the south moat when the rate slowed down in mid-1990 and 1996 [*Langbein et al.*, 1993; *Hill*, 2006].

[7] The fourth episode (1997–1998) began between mid-April and late June 1997 [*Hill et al.*, 2003] as an exponential increase in the deformation rate with a ~60-day time constant [*Newman et al.*, 2001]. The onset of significant microseismcity swarming initiated approximately 2 months after the onset of exponential inflation, similar to the 1989–1990 episode [*Newman et al.*, 2001; *Langbein*, 2003; *Hill*

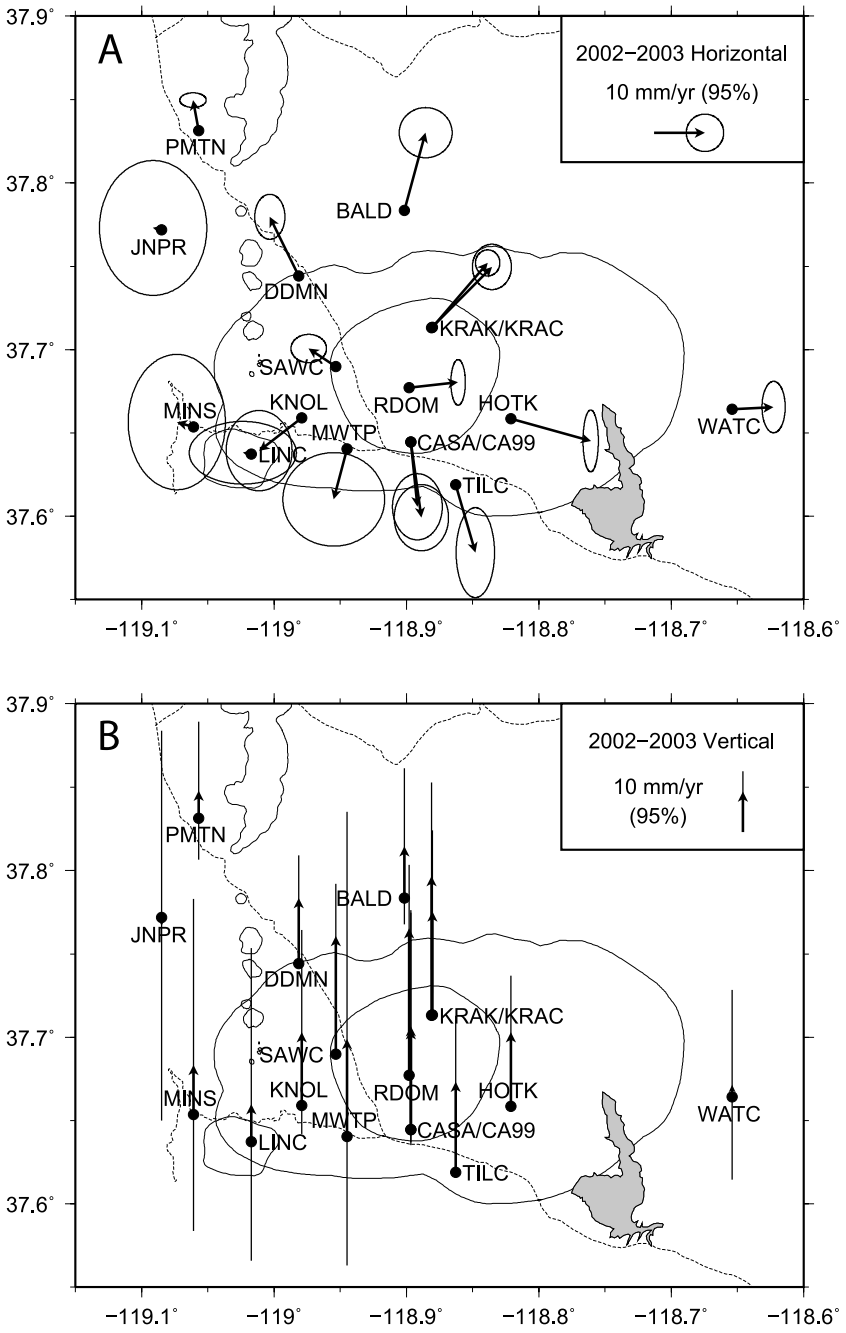

Figure 2. Locations of 17 continuous GPS stations in and near Long Valley Caldera. Arrows show the estimated (a) horizontal and (b) vertical velocities between 2002 and 2003 for all the 17 stations. Ellipses represent 95% confidence error including white noise, flicker noise, and random walk noise.

et al., 2003]. Interestingly, the peak in seismic moment release (in several ~M 5 earthquakes), was coincident with the transition from exponential growth increase, to an exponential growth decay in late November, culminating in approximately 10 cm of uplift [*Newman et al.*, 2001; *Hill et al.*, 2003].

[8] A permanent network of continuous GPS stations, most of which were established in 2000, recorded the most recent episode, which started in early 2002 and ended in early 2003, after a 4-year period of slow subsidence from 1998 through the end of 2001. The accumulative uplift for this episode is ~3.5 ± 0.8 cm estimated from the vertical displacement of site RDOM near the center of the resurgent dome, which compensated and exceeded the previous 4-year subsidence of ~2 cm. Interestingly, no significant increase in seismic activity was observed during this period; however, we detect an opening mode of the Mono-Inyo craters volcanic chain in this period.

[9] The 30 years of observations show uplift and seismicity are not directly coupled neither temporally nor spatially, but do interact with each other. As an example, the 2002–2003 uplift occurred without an obvious increase in seismicity, while a vigorous 1996 earthquake swarm accompanied no uplift. When seismicity and deformation

were observed to be temporally correlated, like the 1989–1990 and 1997–1998 episodes, the onset of an increased seismicity came ~2 months later than the onset of the uplift [*Newman et al.*, 2001; *Langbein*, 2003; *Hill et al.*, 2003]. In examining the occurrence of both seismic increases and periods of quiescence, we find that periods of significant anomalous seismic quiescence occur just prior to the onset of uplift in each of the 1989–1990, 1997–1998, and 2002–2003 episodes.

2. GPS Data and Analysis

[10] A permanent continuous GPS network was established by the United States Geological Survey (USGS) in and around Long Valley beginning in 2000. The new network was established to largely replace the more personnel intensive leveling, trilateration, and EDM surveys. Seventeen GPS stations within and near LVC operated between 2002 and 2003, providing a new and rich data set of three-component time-dependent deformation documenting episodic deformational activity there. The locations of the GPS stations are well distributed: RDOM near the center of the resurgent dome, CASA/CA99 and KRAK/KRAC within the resurgent dome, SAWC near the boundary of the dome, KNOL, MWTP, TILC, HOTK in the moat, DDMN at the rim of the caldera, LINC in Mammoth Mountain, BALD, PMIN, JNPR, MINS, and WATC outside the caldera (Figure 2).

[11] The data were processed using the JPL-GIPSY software, and were obtained from the USGS at http://quake.wr.usgs.gov/research/deformation/gps/auto/LongValley/. The data are reduced to daily positions in the 2000 International Terrestrial Reference Frame (ITRF2000) relative to a stable North American plate. The precision of the data is ~3 mm in horizontal and ~8 mm in vertical. Unfiltered data are available from 1996, while filtered data with the seasonal common mode signal over the regional network removed [*Hammond and Thatcher*, 2007; *Wdowinski et al.*, 1997; *Langbein*, 2008] are available from 2000.

[12] We use the unfiltered data, which extend back to 1996, to establish the baselines between the reference station, KRAK, and other GPS sites (Figure 3). KRAK is the second GPS station installed at LVC after CASA [*Dixon et al.*, 1997] and is much less influenced by the geothermal power production at the Casa Diablo Hot Springs than CASA [*Langbein*, 1989; *Sorey et al.*, 1995; *Howle et al.*, 2003]. Because much of the noise is removed using local baselines, these results can be considered similar to the available filtered results from the USGS. The resulting baseline data show an obvious rapid change in most stations during early 2002 through early 2003. Compared to the exponential uplift in 1997–1998, the 2002–2003 uplift is quite small, about 1/3 of the size.

[13] To get the local deformation of LVC, we further remove the effect of a rigid Sierra Nevada block relative to the stable North American plate from the regionally filtered data using the Euler vector (17.0°N, 137.3°W, rotation rate 0.28°/Ma) defined by *Dixon et al.* [2000]. Transitions associated with the onset and cessation of the most recent uplift episode are gradual and long-lasting and hence are difficult to precisely determine from the daily GPS solutions. Thus, we chose a 1-year time period between 1 January 2002 to 31 December 2002 to roughly represent the episodic uplift event. Further refinement of this episode is not likely because the end points are during a period of significant snow cover, and hence sparse and noisy temporal data coverage. Assuming a constant uplift rate throughout the episode we estimated the approximate linear three dimensional deformation rates using a nonlinear weighted least squares algorithm (T. Williams et al., Gnuplot—An interactive plotting program, Gnuplot manual version 4.2, 2007).

[14] The error estimate of the rate is important for the completeness of rate evaluation and understanding the level of noise. Two error sources commonly associated with GPS are time-uncorrelated white noise and time-correlated colored noise [*Mao et al.*, 1999]. The time-correlated noise can be described by power law models, such that the power density is related to frequency by f^{-n}, where f is frequency and n is the spectral index [*Williams*, 2003; *Langbein*, 2004]. Generally, n is 1 for flicker noise [*Zhang et al.*, 1997; *Mao et al.*, 1999] and 2 for random walk noise [*Langbein and Johnson*, 1997]. A background noise model including white, flicker and random walk noise is used to estimate the standard error in rate. The amplitude of each noise component for all 17 stations is obtained from regionally filtered data between 2000 and 2008 (see Appendix A). The uncertainties for evenly spaced data contributed from white [*Zhang et al.*, 1997], flicker [*Bos et al.*, 2008], and random walk noise [*Zhang et al.*, 1997] are calculated by

$$(\sigma_{\dot{r}})_w^2 = \frac{a_w^2}{T^2}\frac{12(n-1)}{n(n+1)} \approx \frac{12a_w^2}{nT^2} \tag{1}$$

$$(\sigma_{\dot{r}})_{fl}^2 = \frac{8a_{fl}^2}{\pi\Delta T^{\frac{3}{2}}(n^2-n)} \tag{2}$$

$$(\sigma_{\dot{r}})_{rw}^2 = \frac{a_{rw}^2}{T} \tag{3}$$

respectively, where n is the number of data points, T is period of observation in years, ΔT is the sampling period in years; a_w, a_{fl}, and a_{rw} are the amplitudes of white, flicker, and random walk noise, and $(\sigma_{\dot{r}})_w$, $(\sigma_{\dot{r}})_{fl}$. and $(\sigma_{\dot{r}})_{rw}$ are the standard errors in rate from white, flicker, and random walk noise.

[15] The total error of the rate from all the three contributors can be calculated by

$$\sigma_{\dot{r}} = \sqrt{(\sigma_{\dot{r}})_w^2 + (\sigma_{\dot{r}})_{fl}^2 + (\sigma_{\dot{r}})_{rw}^2} \tag{4}$$

The estimates for the displacement rates and 95% confidence errors for the 17 regional GPS sites during 2002–2003 are shown in Figure 2. Most horizontal rates show a radially symmetric pattern about the western part of the resurgent dome, which is attributed to the pressure source beneath LVC. Four stations outside the caldera (PMTN, JNPR, MINS, and LINC) largely deviated from the radial pattern. In the region west of the caldera, the influence of the relatively stronger Sierra Nevada bedrocks (as identified by an increase in seismic P velocity by ~20% in Sierran crystalline bedrock to the south and west of the caldera [*Foulger et al.*, 2003]) are affecting the deformational field, hence these data are removed from analysis to avoid introducing additional errors. All stations are weighted equally

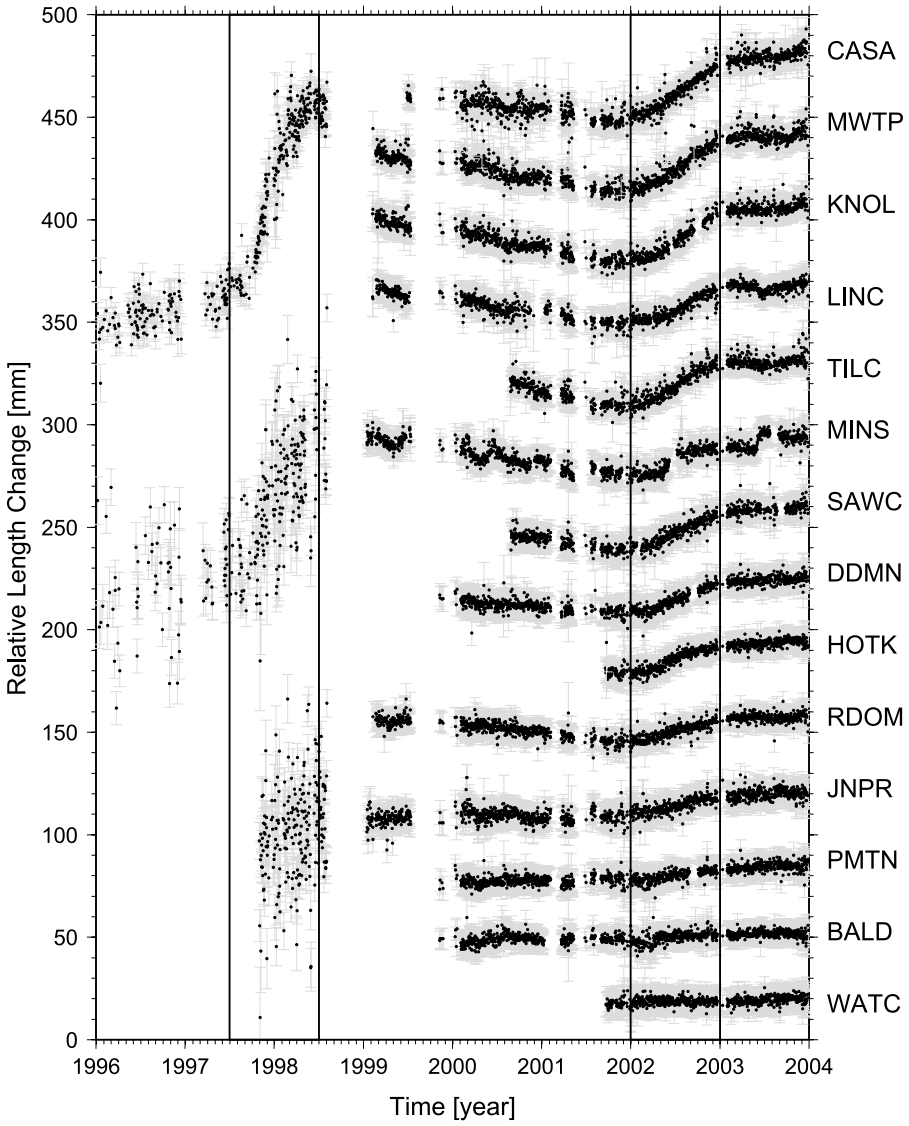

Figure 3. Relative GPS baseline length changes between the reference station, KRAK, and other GPS stations. Most stations show a clear rapid extension during the 2002–2003 period right after a short-term contraction. CASA, MINS, and JNPR, established before 1999, also display a much larger length increase during the 1997–1998 episode.

with the exception of the CASA/CA99 and KRAK/KRAC pairs which were each assigned half weighting to account for collocation.

[16] The maximum uplift of this 2002–2003 episode is approximately $\sim 3.5 \pm 0.8$ cm as determined by uplift at site RDOM, which, as its name suggests, is the closest station to the center of the resurgent dome. This uplift event compensates for subsidence after the 1997–1998 episode, resulting in approximately 80 cm of total uplift since the late 1970s.

3. Analytical Models

[17] Since *Savage and Clark* [1982] performed the first model of a small spherical pressure source [*Mogi*, 1958], hereafter Mogi model, in LVC using leveling data, numerous modeling efforts have been performed on the first four uplift episodes and interim periods. On the basis of these results, two magmatic sources and two seismogenic sources are recognized to have contributed the surface deformation in LVC [e.g., *Hill*, 2006]. The two magmatic sources are a primary inflation source beneath the resurgent dome, and an additional deeper inflation source beneath the south moat. The two seismogenic sources are a set of WNW striking right-lateral faults within the south moat seismic zone (SMSZ), and a set of NNE striking left-lateral faults forming a 10-km-wide zone within the Sierra Nevada block just south of the caldera. The orientations of these two strike-slip fault sets indicate a local ENE extension in LVC [*Hill*, 2006]. The inflation source responsible for the radial symmetric displacement pattern during the 2002–2003 episode is ~ 3 km west of the central resurgent dome, and is consistent with the primary inflation source from the previous episodes and interim periods. No contribution from a secondary source was resolved during the 2002–2003 episode, possibly due to the reduced magnitude of overall inflation compared to previous episodes. No long-term increase in earthquake

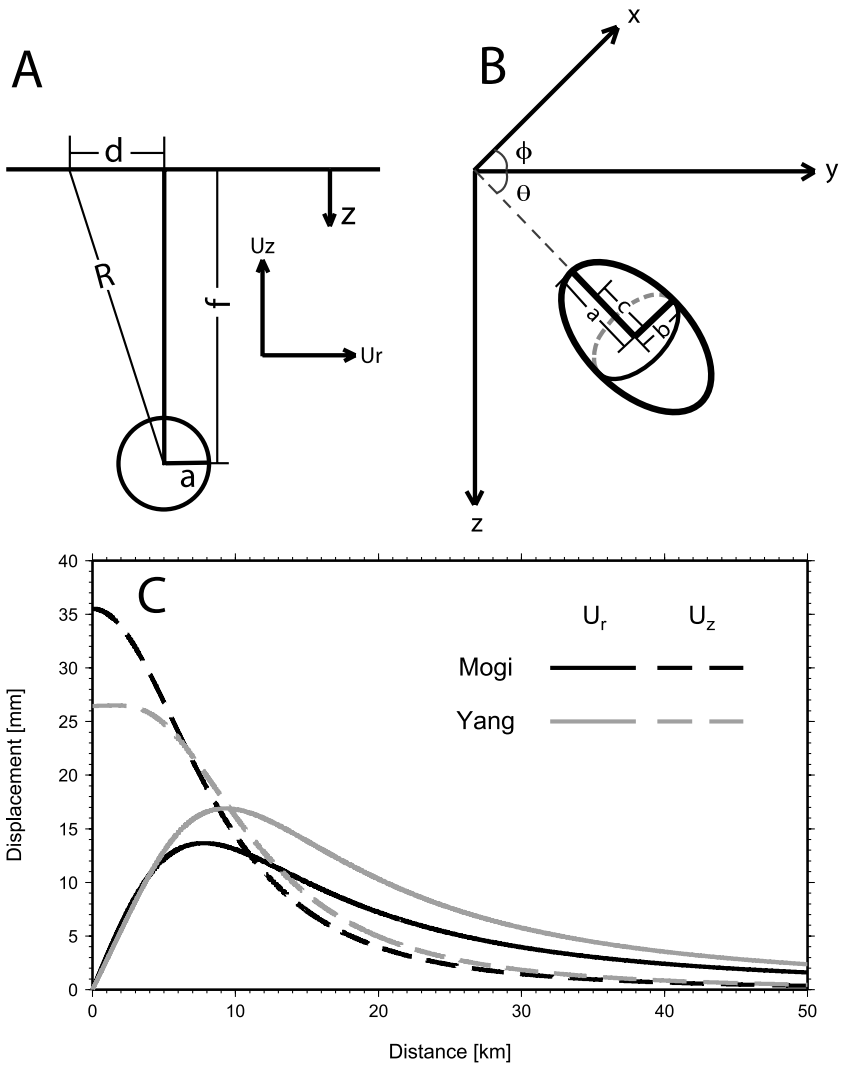

Figure 4. Schematic characterization and coordinate systems for the analytic Mogi and Yang models. (a) Mogi model: a and f are the radius and depth of the sphere, d and R are the horizontal and linear distance to the center of the sphere satisfying $R^2 = d^2 + f^2$. (b) Yang model: a and b are the semimajor and semiminor axes, c is the distance from center to focus satisfying $a^2 = b^2 + c^2$, θ and ϕ are the dip and azimuth of the spheroid. (c) Vertical and radial displacements away from a Mogi source (at z = 11 km, $\Delta V = 0.018$ km^3), and a vertically dipping Yang source (at $z = 9.6$ km, $\Delta V = 0.021$ km^3, $b/a = 0.5$) models.

activity, or large individual earthquakes (largest M = 3.2) were observed during this period, thus slip-induced deformation along the south moat is not significant during this time.

[18] The source of previous inflation episodes has been suggested to be a combination of partially molten magma and hydrous fluids [*Hill*, 2006], and there is no evidence to suggest this episode is different. The existence of partial melt at shallow depths in the LVC is supported by the volcanic history of LVC [*Bailey et al.*, 1976; *Bailey*, 1989], the seismic refraction data [*Hill*, 1976; *Hill et al.*, 1985], the tomographic inversions [*Dawson et al.*, 1990; *Steck*, 1995; *Sanders et al.*, 1995; *Weiland et al.*, 1995], and strongly suggested by changes in gravity associated with the 1997–1998 episode [*Battaglia et al.*, 1999].

[19] A simple Mogi model is first tested to locate the inflation source by fitting the GPS data. The Mogi model is an analytic solution for a spherical pressure source, which represents a uniformly pressurized spherical cavity in a homogeneous elastic half-space, and is valid for a relatively small radius compared to its depth [*Mogi*, 1958] (Figure 4a). With the pressure P replaced by the volume change ΔV and the source radius a using the relation $P = \mu \Delta V / \pi a^3$ [*McTigue*, 1987], the number of free parameters can be reduced to four (3 components of source location, and volume change). To more fully describe the field of potential source locations, we used a grid search across a wide range of the four parameters to find the best fit models utilizing all three components of observed deformation. The best fitting solutions was determined from the combination of parameters that minimized the reduced chi-square, χ_r^2 (similar to that of *Newman et al.* [2006]). Because χ_r^2 accounts for complexity of the input model, by reducing the weighted sum of the squared residual by the degrees of freedom,

Table 1. Summary for Models Including 95% Likelihood Range as Determined by Bootstrap[a]

Model	ndf	χ^2	χ^2_r	Longitude (deg)	Latitude (deg)	Depth (km)	ΔV (km^3)	b/a
No model	33	1534.55	46.50					
Mogi	29	56.72	1.96	−118.930	37.678	11.7	0.023	
				−118.935 to −118.908	37.672–37.687	7.5–13.5	0.010–0.030	
Yang	28	52.83	1.89	−118.931	37.678	10.6	0.022	0.76
				−118.936 to −118.910	37.672–37.686	9.2–12.2	0.015–0.027	0.55–0.99

[a]Here ndf is number of degrees of freedom.

it is also a good indicator of the appropriateness of a given model, such that a result that approaches 1.0 theoretically has both an ideally suited model, and appropriately determined errors [*Press et al.*, 1992].

[20] Because of its simplicity, the Mogi model is a useful tool for initially assessing the location and approximate magnitude of an inflation source. However, it is appropriate to assess other models that may more accurately characterize the nature of the source or rheology, if adequate spatially dense data are available. The vertically dipping prolate spheroid model [*Yang et al.*, 1988], hereafter Yang model, has been found to more adequately characterize the deformation sources from the previous episodes [*Fialko et al.*, 2001; *Battaglia et al.*, 2003a, 2003b; *Langbein*, 2003], therefore we additionally test its utility for the 2002–2003 episode. The Yang model was developed as an arbitrarily dipping finite prolate spheroid pressure source model, which represents a uniformly pressured arbitrarily oriented prolate spheroid cavity of finite dimensions in a homogeneous elastic half-space (Figure 4b). With the substitution of $\mu\Delta V/\pi ab^2$ for P, where ΔV is the volume change, a is the semimajor axis, b is the semiminor axis, and μ is the shear modulus [*Tiampo et al.*, 2000], the Yang model requires seven free parameters to calculate the displacements at surface for a Poisson's solid (source location, volume change, axis ratio (b/a), and the dip and azimuth of the spheroid). Because previous models do not require a significant dip on the prolate spheroid geometry, we thus hold it fixed thereby removing two parameters (dip and azimuth). Similar to the method used for solving the Mogi model, we applied a grid search across a range of the remaining five free parameters to find the best fit parameter combination. While the overall shape of deformation is similar between the Mogi and a vertically dipping Yang model, subtle differences in the shape of both vertical and radial deformational fields increase as the Yang model becomes more prolate (Figure 4c).

4. Model Results

[21] The parameters of the best fit Mogi and Yang models are summarized in Table 1. Both best fit models explain up to 96% of the surface deformation. The χ^2_r of both is about 1.9, suggesting our simple analytical models are appropriate for the observed deformation and the errors are realistic. While the χ^2_r of the Yang solution is fractionally smaller than the Mogi solution, it is difficult to argue that it is enough to compensate for the increased model complexity. An F test is used to test whether the Yang model is significantly superior to the Mogi model (e.g., H. J. Motulsky and A. Christopoulos, Fitting models to biological data using linear and nonlinear regression. A practical guide to curve fitting, GraphPad Software Inc., San Diego, California, 2003, available at http://www.graphpad.com). F is defined as

$$F = \frac{\left(\chi^2_{Mogi} - \chi^2_{Yang}\right) / \left(ndf_{Mogi} - ndf_{Yang}\right)}{\chi^2_{Yang} / ndf_{Yang}} \tag{5}$$

where χ^2 is chi-square, also known as the weighted sum of the squared residuals (WSSR), ndf is the number of degrees of freedom.

[22] We find an F ratio of 2.06 corresponding to a 16% likelihood that the improved fit is from random chance; hence either model may be considered appropriate for this episode. Both models suggest a similar source location and volume change, and because Yang model axis ratios near 1 (optimal b/a = 0.76), that of a sphere, thus the source geometry can also be considered highly similar. The volume change for this 1-year period, ~0.02 km^3, is comparable to ~0.03 km^3 from previous studies; however, the depth from this study is 11 km and is somewhat deeper than ~7–8 km suggested for previous sources.

[23] To test the sensitivity of best fit results to the change in model parameters, we fix either the horizontal position or the depth and volume change (and axis ratio for Yang model) at the best fit values to determine the chi-square distribution of the remaining parameters. The best fit locations are well constrained (Figures 5a and 6a); however, a trade-off between depth, volume change, and ellipticity exists (Figures 5b, 6b, and 6c).

[24] To better assess the range of possible solutions dependent on station availability, we use a bootstrap method, randomly subsetting the data for both the Mogi and Yang models. For each of 10,000 iterations, 11 of 13 station locations were randomly selected and best fit locations were subsequently identified. Station pairs CASA/CA99 and KRAK/KRAC were colocated, and hence were treated as 1 location each. The distribution of best fit determinations yields a robust assessment of the probability distribution of the parameters for a given model. For the Mogi solution, we allow the four parameters (latitude, longitude, depth, and volume change) to vary simultaneously. However, for the Yang solution we preferred to utilize a two-step process, first fixing the axis ratio (b/a) at the best fit value to determine the simultaneous range of the horizontal position. Subsequently, we hold the horizontal position fixed at the best fit value and determine the parameter range for depth, axis ratio and volume change, for which there is a trade-off. The variability in each parameter is shown in Figures 5c–5f and 6d–6h. The 95% confidence is given in Table 1.

[25] The model displacements are generally consistent with the GPS observations (Figures 7a and 7b), except at

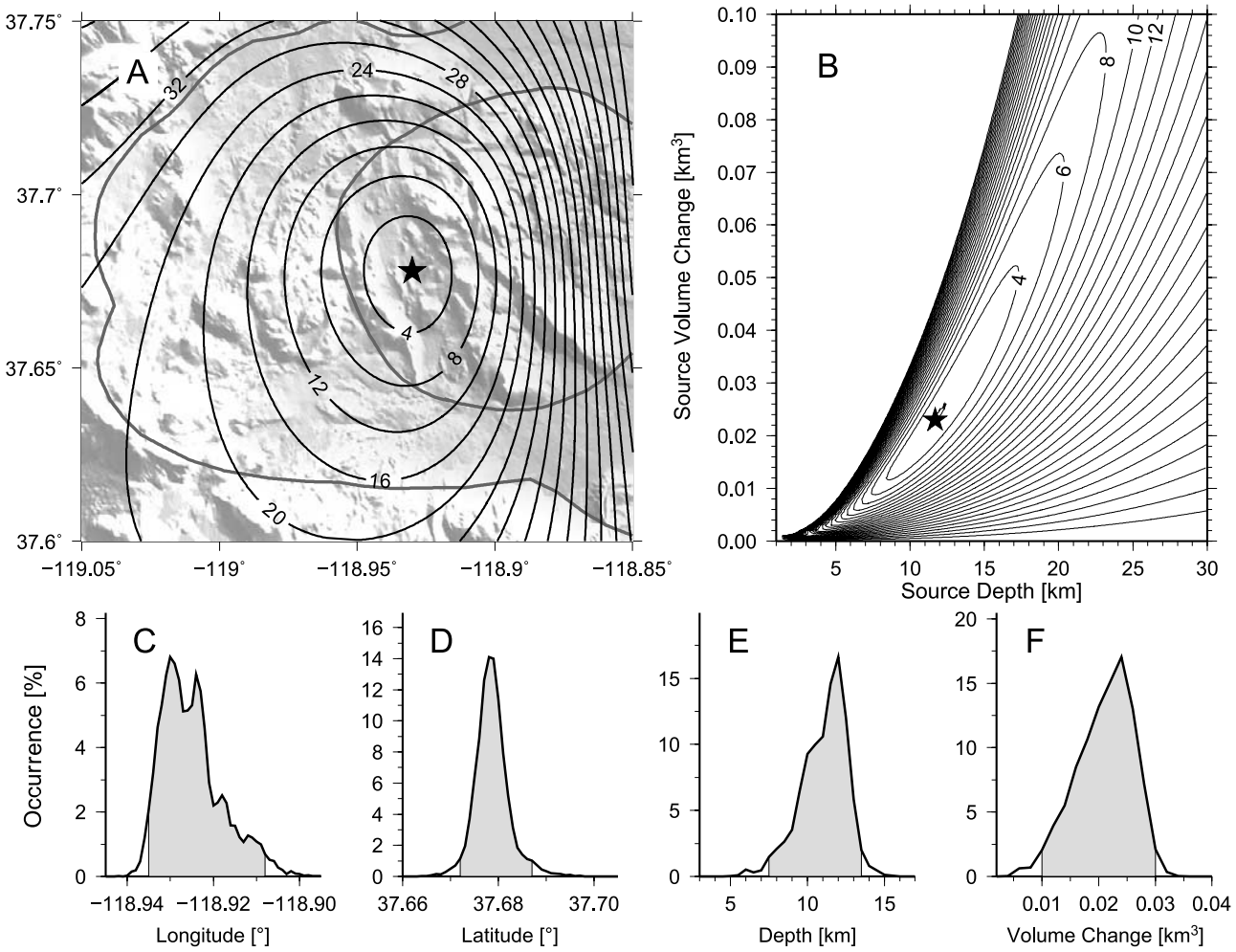

Figure 5. Mogi models for the 2002–2003 episode. (a and b) Contours of χ_r^2 for the pair of longitude and latitude and the pair of source depth and volume change. Stars indicate the best fit parameters. (c, d, e, and f) Histograms of best fit values from 10,000 bootstrap runs for the source longitude, latitude, depth, and volume change. The vertical lines show the 95% confidence level.

the four stations that were excluded from the model determinations (PMTN, JNPR, MINS, and LINC). The models overpredict deformation at these stations presumably because the Sierra Nevada bedrock west of the caldera is stronger (tomography from *Foulger et al.* [2003]), and hence dampens the deformation outside the caldera.

[26] The residual velocities (Figures 7c and 7d), which are obtained by subtracting the model prediction from the data, show some interesting features. The residuals of five station locations (BALD, KRAK/KRAC, RDOM, WATC, and MWTP) toward NE to ENE direction are consistent with the local ENE background extensional direction [*Prejean et al.*, 2002; *Hill*, 2006], while the residuals of three stations (DDMN, SAWC, and KNOL) shift 90° toward the SE direction potentially influenced by transient activity along the Mono-Inyo chain (see section 5). CASA/CA99 located 1 km east of the Casa Diablo geothermal well field has been pulled westward at a rate of 3–5 mm/a by the local subsidence of the well field [*Sorey et al.*, 1995; *Howle et al.*, 2003; *Langbein*, 2003], which could explain why the residual motion of CASA/CA99 does not correspond with the observed NE-ENE extension.

5. Discussion

5.1. Opening Mode of Mono-Inyo Craters

[27] Adjacent to LVC is both Mammoth Mountain and Mono-Inyo craters (Figure 1). These volcanoes form a 45-km-long north trending volcanic chain west of, and extending north of the caldera. Petrologic results show that these two systems are compositionally distinct from LVC [e.g., *Bailey*, 1989; *Kelleher and Cameron*, 1990]. While the chain penetrates the topographic boundary of Long Valley, the system lies outside the inferred ring faults of the caldera [*Suemnicht and Varga*, 1988; *Hildreth*, 2004], and therefore they may derive from younger magma chambers not directly related to Long Valley chamber [*Bailey*, 1989; *Hildreth*, 2004; *Hill*, 2006]. However, the interrelation between the two systems is still not well known.

[28] In examining details of the eastern component of the GPS time series for baselines of sites that cross the Mono-

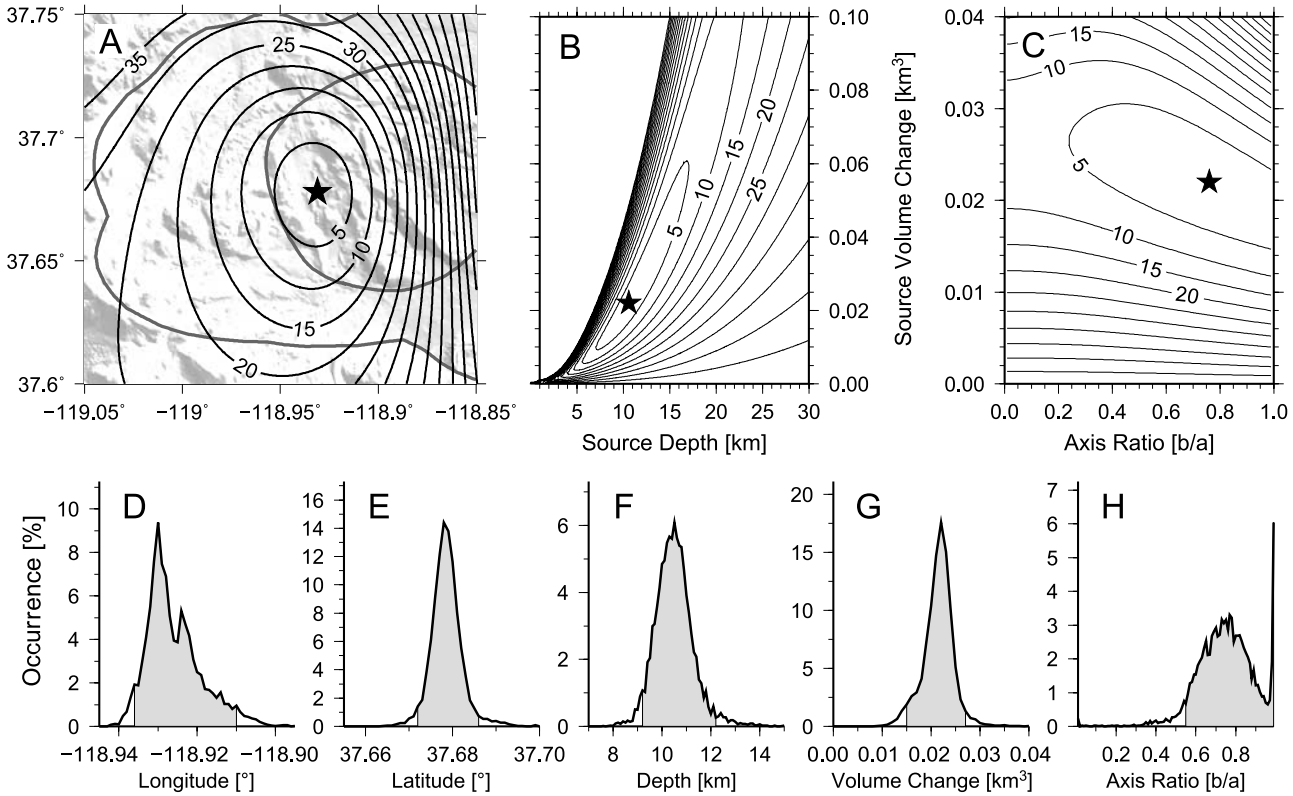

Figure 6. Same as Figure 5 but for prolate spheroid Yang models for the 2002–2003 episode. (a, b, and c) Contours of χ_r^2 for the pair of longitude and latitude, the pair of source depth and volume change, and the pair of axis ratio and source volume change. Stars indicate the best fit parameters. (d, e, f, g, and h) Histograms of best fit values from 10,000 bootstrap runs for the source longitude, latitude, depth, volume change, and axis ratio. The vertical lines show the 95% confidence level.

Inyo chain, we identify a distinct change in the opening rate associated with the 2002–2003 uplift at LVC. Four stations with high-quality data are available near the Mono-Inyo chain spanning from late 1999 to either mid-2007 or present: PMTN, JNPR on the west side and BALD, DDMN on the east side (Figure 8a). P648-P632 (Figure 8a), a pair of plate boundary observatory (PBO) sites available from late 2006 are also included. The east-west component of the unfiltered GPS data is used to form five east-west baselines (Figure 8c). Linear changes in the east-west baselines were determined using maximum likelihood estimator (MLE) [*Langbein*, 2004, 2008] for three periods: the 2002–2003 inflationary episode, the preinflationary period including all available data after the 1997–1998 episode, and the post-inflationary period, including all available data beginning in 2003 to mid-2007 when data were available for all the baselines, and are summarized in Table 2 with their standard errors (1σ).

[29] For both the preinflationary and postinflationary periods, rates were positive showing that sites to the east are moving more eastward relative to those in the west, which can be interpreted as an opening mode of the Mono-Inyo chain. *Marshall et al.* [1997] similarly identified a possible Mono craters dike opening from a 5-year campaign GPS survey in 1990–1994. During 2002–2003, all eastward baselines were dominated by the uplift. After 2003, the rates again become constant, but at rates higher than those observed before 2002. To test whether the rates before 2002 are statistically significant from those after 2003, we apply a large-sample Z test for parallelism of the two lines [*Kleinbaum and Kupper*, 1978]. We first assume the slopes (rates) before 2002 and after 2003 are essentially the same as the null hypothesis and then test the probability of this assumption. Z is defined as

$$Z = \frac{\dot{u}_{eb} - \dot{u}_{ea}}{\sqrt{S^2_{\dot{u}_{eb}} + S^2_{\dot{u}_{ea}}}} \tag{6}$$

where $\dot{u}_{eb}$ and $\dot{u}_{ea}$ are the slopes/rates before 2002 and after 2003, $S^2_{\dot{u}_{eb}}$ and $S^2_{\dot{u}_{ea}}$ are the variances of the estimated slopes, calculated by

$$S^2_{\dot{u}_e} = \frac{S^2_{Y \cdot X}}{(n-1)S^2_{XX}} \tag{7}$$

where n is the number of data points, $S^2_{Y \cdot X}$ is the residual mean square, S^2_{XX} is the variance of the independent variable X.

[30] Z, which corresponds to one p value, should have a normal distribution with zero mean and unit variance. If $p = 0$, then there is statistically zero chance of the two data sets having the same slope. In examining early and late eastward baseline, we find that p values are less than 10%

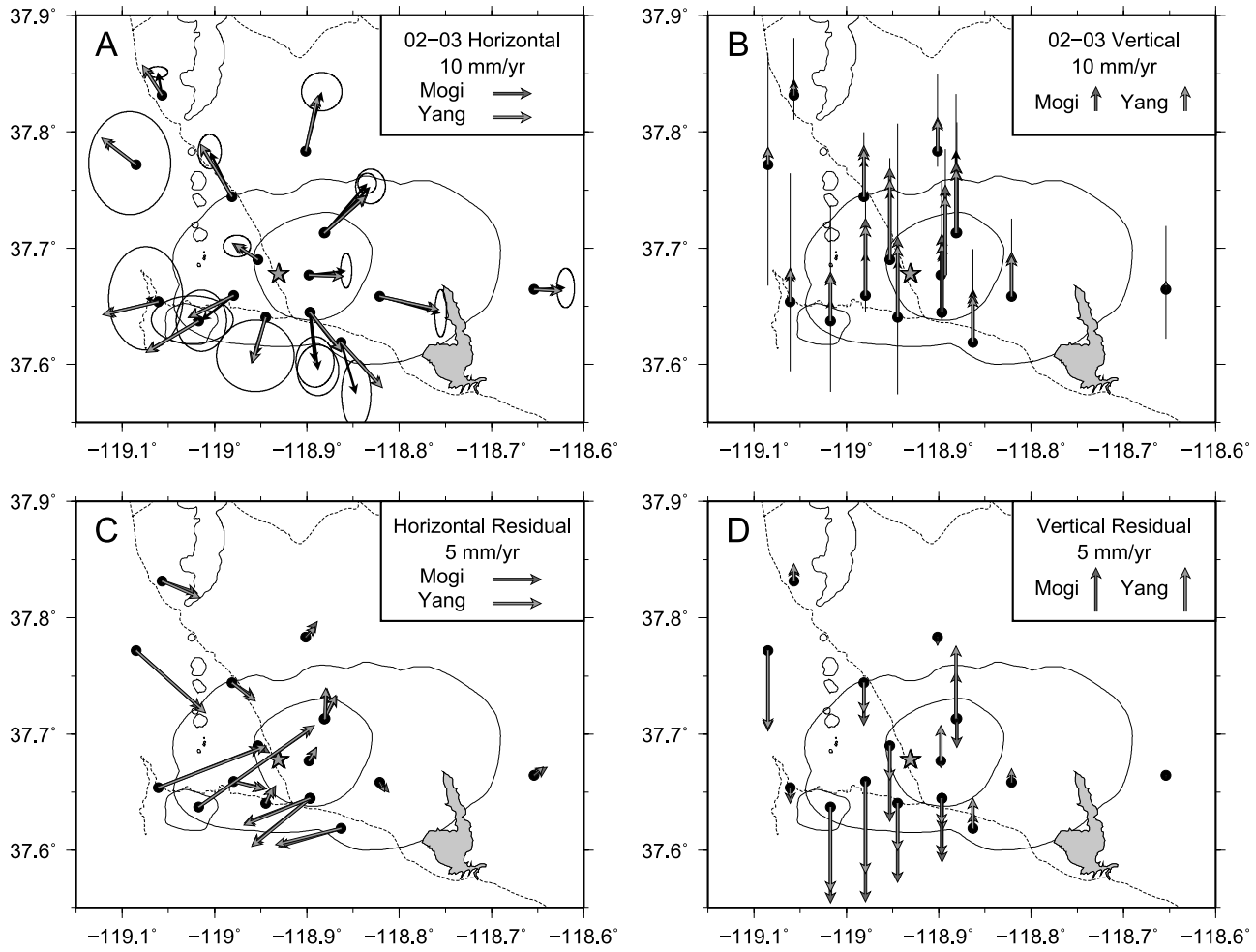

Figure 7. GPS and model (a) horizontal and (b) vertical velocities. Black vectors with error ellipses are observed GPS rates. Model (c) horizontal and (d) vertical residuals. Dark gray and light gray vectors are predicted from the best fit Mogi and Yang models, respectively. Dark gray and light gray stars show the best fit location for the Mogi and Yang model.

for all but one baseline, where p value is 18% (Table 2). Thus, extension rates across the Mono-Inyo chain before 2002 are statistically smaller and different than after 2003. Hence, the increased regional opening is likely real. We postulate that the change in rates is likely associated with either increases in the crustal elastic stress due to the increased inflation, or to interactive fluid pathways at depth that are common to both the resurgent dome and the Mono-Inyo chain. The same methodology was applied to north baselines: While the north DDMN-PMTN baseline rate was determined to be different at 95% confidence, the Z test showed 30%, 38%, and 94% likelihood that differences were due to random variability for the pairs BALD-PMTN, DDMN-JNPR, and BALD-JNPR. Because the Mono-Inyo chain is north trending, along with the subsurface dike [*Fink*, 1985], extension is expected to be primarily east-west, and hence we do not further consider the ambiguous north-south baselines here.

[31] We examined the relative contribution of the recent transient inflation episode at Long Valley on the overall strain field of the Mono-Inyo chain using the six possible baselines resolved from four stations in the region (PMTN, JNPR, BALD, and DDMN; Figure 8a). We separately examined the preinflation (2000–2002), coinflation (2002–2003), and postinflation (2003–2007). For each period we use subsets of three nonparallel baselines (avoiding subparallel pairs BALD-PMTN – DDMN-JNPR, and BALD-DDMN – PMTN-JNPR) to identify 12 sets of principle horizontal strain directions with their individual and average maximum extension directions, shown in Figure 8b (following *Turcotte and Schubert* [2002]). The maximum horizontal extension directions during the inflationary period are in good agreement with each other, and the average is trending N48E, and can be described mostly from inflationary strain from the SE. However, horizontal strains determined before and after the inflationary episode are rotated by approximately 90°, with average maximum extension at S45E and S52E, respectively. The extension direction for these periods are in good agreement with the expected regional strain field north of the caldera due to the confluence of Sierra Nevada Block and Basin and Range extension [*Bursik and Sieh*, 1989; *Prejean et al.*, 2002]. Over the past 40,000 years, *Bursik and Sieh* [1989] suggest that ~1 mm/a of E-W extension is accommodated along the

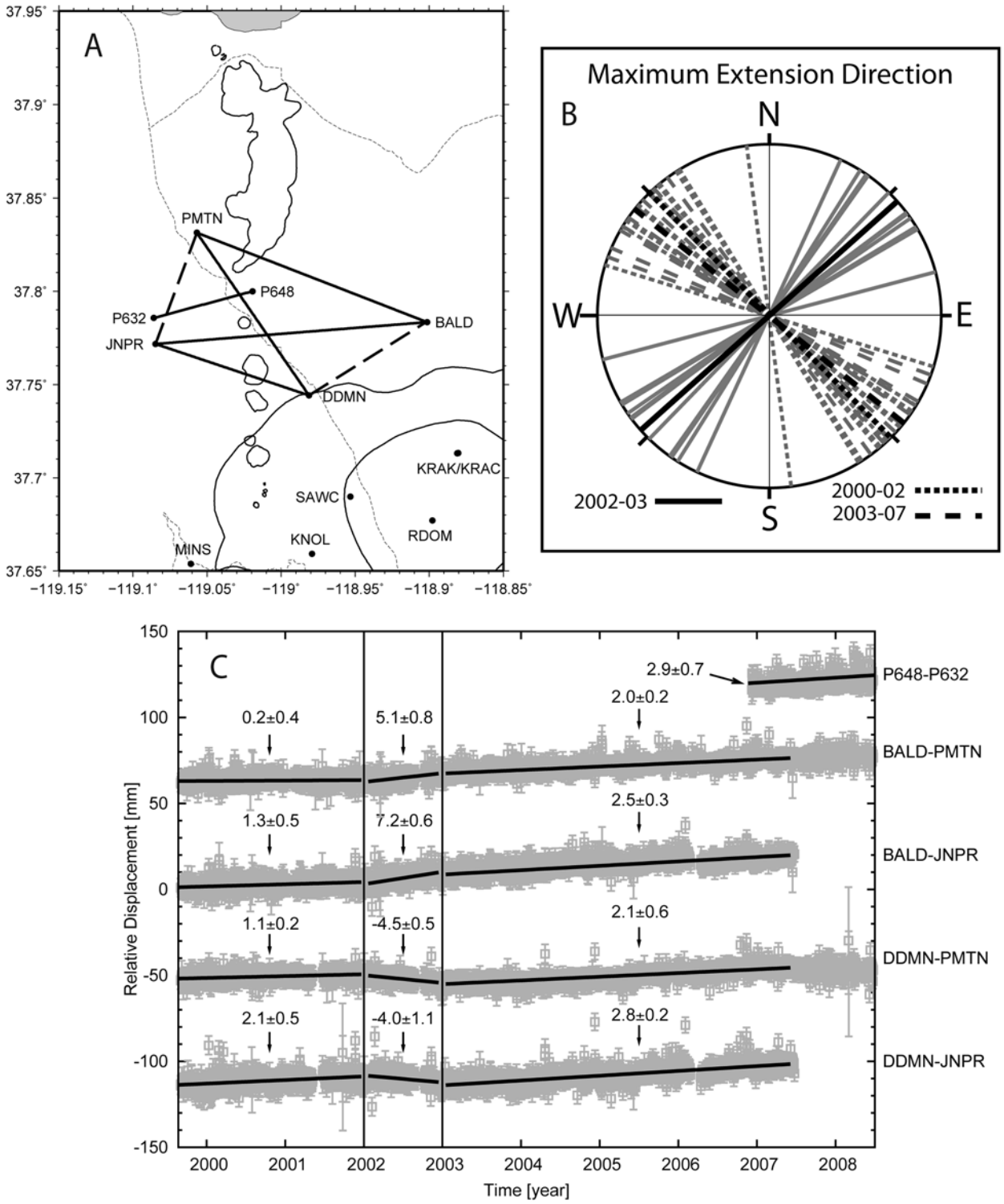

Figure 8. (a) GPS baselines across the Mono-Inyo craters chain. Baseline P632-P648 is used only for qualitative comparison. (b) From baselines (solid and dashed lines in Figure 8a), the individual (gray) and average (black) maximum extension directions are shown for the three periods of observation. (c) East-west component of baselines crossing the volcanic chain (black lines in Figure 8a). Eastward extension rates (mm/a) with standard errors are estimated using the maximum likelihood estimator (MLE) [*Langbein*, 2004, 2008]. Gray bars are GPS data with errors. Thick solid lines are best fit. Positive rates indicate an increase in the east-west extension between sites.

Table 2. East-West Extensional Rates Before 2002 and After 2003

Baselines	Before 2002 (mm/a)	After 2003 (mm/a)	Z Value	p Value
BALD-PMTN	0.24 ± 0.36	2.03 ± 0.17	4.47	0
BALD-JNPR	1.28 ± 0.49	2.54 ± 0.29	2.24	0.03
DDMN-PMTN	1.07 ± 0.21	2.15 ± 0.55	1.83	0.07
DDMN-PMTN	2.09 ± 0.46	2.79 ± 0.25	1.35	0.18
P648-P632		2.91 ± 0.74		

Mono-Inyo dike system. These modern results of between 1 and 3 mm/a observed here are comparable, but show extension to variable, both in direction and magnitude.

5.2. Seismic Indicators of Deformation Change

[32] Increased seismicity occurring approximately 2 months after the onset of inflation has been reported in both the 1989–1990 and 1997–1998 episodes [*Langbein et al.*, 1993; *Dixon et al.*, 1997; *Newman et al.*, 2001; *Langbein*, 2003; *Hill et al.*, 2003]. The seismicity, which is thought to be an expression of a transition in the Eastern California Shear Zone, is predominantly along the south moat and other faults south of the caldera, and not collocated precisely with the inflationary source. However, changes in crustal stress due to caldera inflation undoubtedly have an effect on seismic activity, and may act to either increase activity by increasing shear stress along faults, or decrease it by increasing fault normal stresses. A precise determination of which of these is dominant requires a careful examination of relative fault orientations to the pressure source, and characterization of the stress changes along structural and strength boundaries (e.g., along ring boundaries).

[33] While such a characterization is beyond the scope of this paper, we empirically advance the observed relationship between the resurgent dome uplift and predominantly south moat seismicity. The earthquake data within the larger SMSZ (confined by the lower left point [−119.00°,

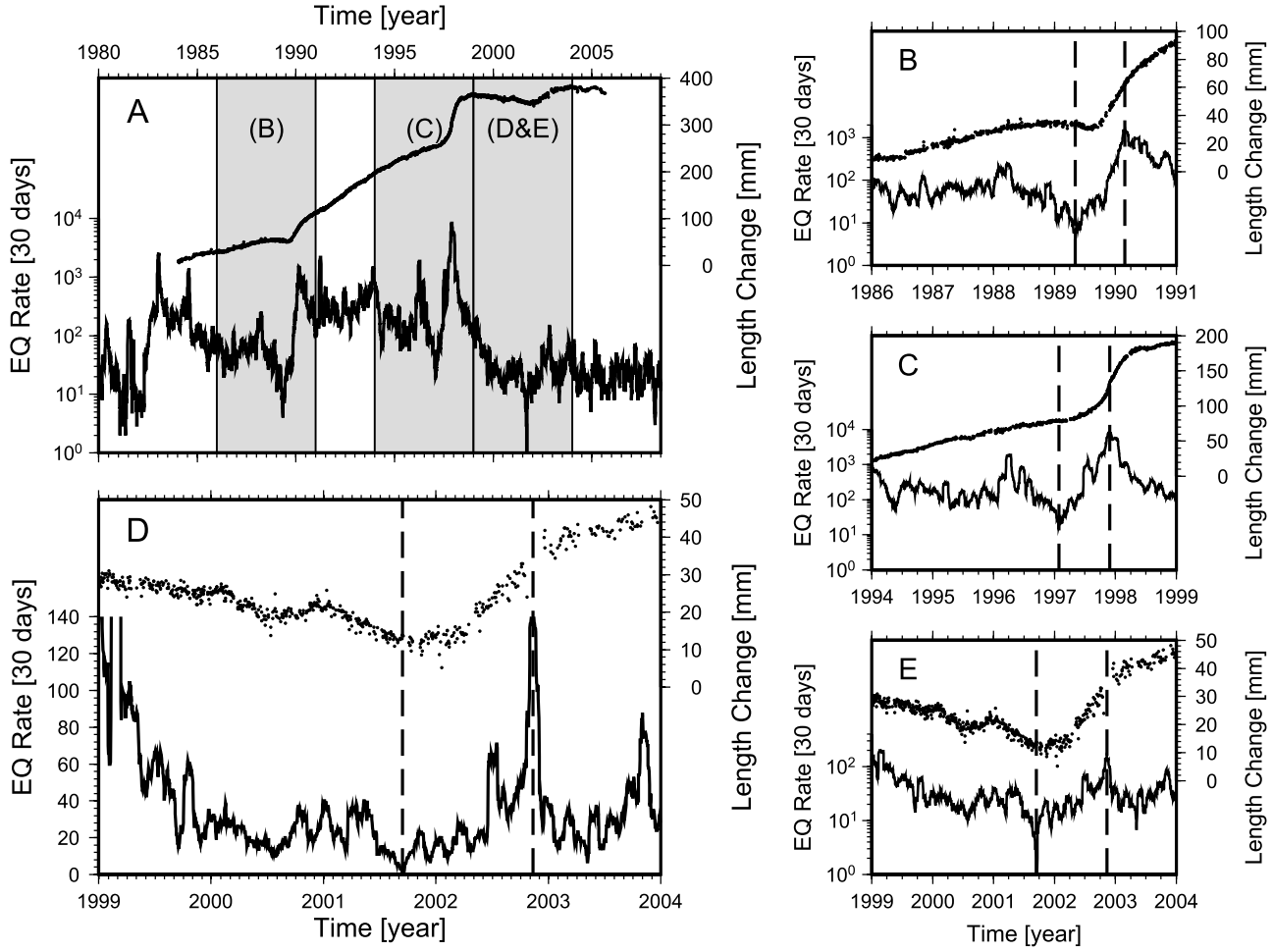

Figure 9. Black lines are 30-day centrally averaged earthquake rates in the larger South Moat Seismic Zone (SMSZ). Black dots are normalized EDM baselines between CASA and KRAK. (a) In 1980–2006. Gray boxes highlight the periods for Figures 9b, 9c, 9d, and 9e. (b) In 1986–1991. (c) In 1994–1999. (d and e) In 1999–2004 (linear and log earthquake rates). The first dashed line in Figur es 9b, 9c, 9d, and 9e indicates seismic quiescence immediately prior to inflation, while the second dashed line indicates the peak in seismic activity during the maximum rate of uplift.

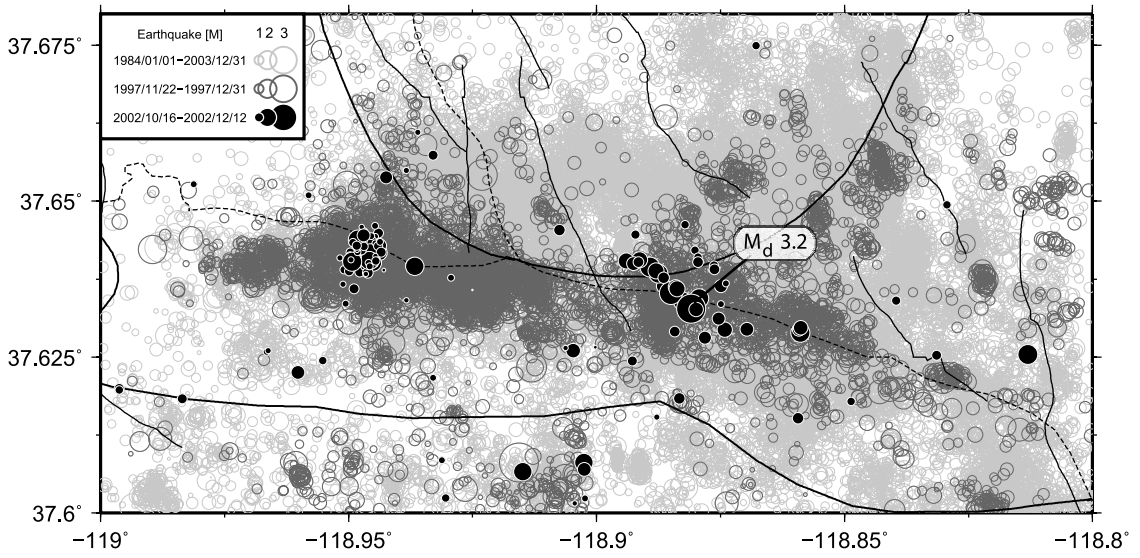

Figure 10. Seismicity in the larger SMSZ area between 1984 and 2003. Dark gray open circles represent earthquakes during the seismic peak of the 1997–1998 episode. Black solid circles indicate earthquakes during the seismic peak of the 2002–2003 episode. Light gray circles are other earthquakes in 1984–2003.

37.60°] and the upper right point [−118.8°, 37.68°]) from 1980 to mid-2008 are from the Northern California Seismic Network (NCSN) catalog (http://www.ncedc.org). While long-term changes in seismicity rate may occur from network changes, likely causing an increased observation bias with time, the short-term changes of interest are largely unaffected. We use a 30-day sliding window with 1-day step to compute the average activity. We compare these results to the CASA-KRAK EDM baseline, because it is the only continuous deformational data set available for each episode examined (1989–1990, 1997–1998, and 2002–2003; Figure 9).

[34] For all episodes, including 2002–2003 an episode with no large long-term increase in background seismicity, we observe a clear peak in seismicity during the maximum rate of uplift. The maximum periods of activity are shown against all SMSZ activity between 1984 and 2003 (Figure 10). Seismicity catalog used here are relocated using waveform cross-correlation and double-difference methods, yielding improved hypocenter locations [*Waldhauser and Schaff*, 2008]. While seismicity is somewhat distributed spatially over the 20-year period, activity occurs predominantly along the SMSZ during both the 1997 and 2002 peaks in activity. During these peaks, not surprisingly, the largest earthquakes also occur: A series of $M_W \sim 4.8$ events occurred in late November 1997, and an $M_d = 3.2$ occurred in early November 2003, all along the south moat.

[35] More surprisingly, we identified a uniquely anomalous seismic quiescence immediately prior to the onset of uplift during each episode. For each episode the seismic activity was at its absolute lowest in several years, immediately before an episode of uplift is observed. The decrease in seismicity for each quiescent period is actually lower than at any other time since the onset of the previous uplift event. For the 2002–2003 episode, only one earthquake was recorded in SMSZ for a 30-day period, while for the preceding several years, between 20 and several hundred events were recorded monthly.

6. Conclusion

[36] The most recent 2002–2003 uplift is part of the remarkable continued episodic dome growth at Long Valley Caldera that began in the late 1970s. This most recent period is similar to previous episodes of 1979–1980, 1983, 1989–1990, and 1997–1998. A total uplift of ~80 cm has accumulated on the resurgent dome. The 2002–2003 episode is responsible for ~3.5 ± 0.8 cm of uplift, which is about 1/3 the magnitude of the 1997–1998 episode, but with a similar exponential shape. Whether the continued uplift over the past 25 years is a long-term transient (e.g., tumescence), or permanent dome growth due to magmatic intrusion remains unclear.

[37] Similar to previously observed episodes of inflation, uplift between 2002 and 2003 is primarily radial, and can largely be explained by a compact inflation source located ~3 km west of the central resurgent dome. Spherical Mogi models and vertically dipping prolate spheroid Yang models are chosen to constrain the source location and geometry. For the Mogi source, the optimal source is located at −118.930°, 37.678°, and approximately 11 km depth. A trade-off between depth, volume change is observed, thus a depth range between 7.5 and 13.5 km and a volume change of 0.01–0.03 km^3 is observed at 95% confidence. The location and volume change for the Yang model are indistinguishable from Mogi model; however, a modest stretching of the source is preferred over the spherical Mogi geometry (b/a = 0.76). Both Mogi and Yang models explain up to 96% of the deformation characterized by the three orthogonal components of 13 continuous GPS stations. A small reduction of WSSR suggests a slight but potentially insignificant preference for the prolate spheroid Yang model.

Table A1. Estimated Amplitudes for the Regionally Filtered Data of 17 GPS Sites in and Near Long Valley Caldera Between 2000 and 2008

	North			East			Up		
Site	a_w (mm/a)	a_{fl} (mm/a$^{0.25}$)	a_{rw} (mm/a$^{0.5}$)	a_w (mm/a)	a_{fl} (mm/a$^{0.25}$)	a_{rw} (mm/a$^{0.5}$)	a_w (mm/a)	a_{fl} (mm/a$^{0.25}$)	a_{rw} (mm/a$^{0.5}$)
BALD	1.10	1.89	1.82	1.03	2.11	0.50	3.75	7.78	1.50
CA99	1.50	2.53	2.08	1.25	1.91	1.50	4.01	10.8	11.60
CASA	1.50	2.53	2.10	1.22	2.14	1.00	4.04	10.79	11.90
DDMN	1.06	1.71	1.50	1.38	1.05	1.50	4.06	0.31	11.49
HOTK	1.38	2.41	1.50	1.08	0.01	1.59	3.92	5.56	1.50
JNPR	1.74	5.39	1.00	1.72	4.26	1.50	4.68	19.54	1.50
KNOL	1.06	3.17	1.50	1.19	2.58	1.50	3.63	10.11	3.76
KRAC	1.18	0.80	1.75	1.23	0.78	1.50	4.28	7.83	6.03
KRAK	1.16	1.70	1.70	1.28	1.45	1.50	4.31	9.10	5.90
LINC	1.43	2.44	1.50	1.33	4.26	1.50	3.41	15.28	9.65
MINS	0.47	5.42	1.00	1.01	3.22	5.99	2.33	16.65	1.50
MWTP	1.41	3.61	2.73	1.44	4.04	1.50	3.77	22.45	10.16
PMTN	1.13	0.03	1.50	1.44	0.87	1.50	4.05	6.85	1.50
RDOM	1.09	1.81	0.50	1.04	0.01	1.50	3.56	5.83	6.84
SAWC	1.12	1.10	0.50	1.16	1.30	1.50	4.32	4.99	3.92
TILC	1.78	3.48	2.46	1.30	1.23	2.45	4.92	6.55	1.94
WATC	0.96	2.05	0.50	0.92	0.84	1.00	3.58	9.47	1.50

[38] A significant increase of 1–2 mm/a in the rate of opening of the Mono-Inyo volcanic chain is associated with the 2002–2003 uplift of LVC, as identified by changes in east-west baselines across the chain. This result suggests that the inflation within the resurgent dome of Long Valley Caldera, and activity along the Mono-Inyo craters are linked either by transmitted elastic stresses in the crust or by connectivity of deeper fluid pressures in the magmatic plumbing system.

[39] Changes in the crustal stress regime immediately prior to and during the maximum rate of uplift may additionally be responsible for significant and consistent changes in the rate of seismic activity along the South Moat Seismic Zone. This is suggested by the observation that peak seismicity rates coincides with maximum inflation rates–well after uplift begins. Similarly, a significant episode of seismic quiescence is identified immediately prior to the onset of the uplift in each of the 1989–1990, 1997–1998, and 2002–2003 episodes.

Appendix A

[40] Estimated amplitudes for white a_w, flicker a_{fl}, and random walk a_{rw} noise for the regionally filtered data of 17 GPS sites in and near Long Valley Caldera (LVC) between 2000 and 2008 (J. Langbein, personal communication, 2009) are given in Table A1. Amplitude solutions are determined following the maximum likelihood estimator (MLE) methodology described by *Langbein* [2004].

[41] **Acknowledgments.** We are highly appreciative of J. Langbein and an anonymous reviewer for careful and insightful reviews. We also thank Langbein for supplying improved individual station error modeling for this study. Most figures were developed using the freely available Generic Mapping Tools (GMT) [*Wessel and Smith*, 1991]. This project benefited greatly from the readily available and easy-to-use GPS and EDM processed data products supplied by U.S. Geological Survey for the Long Valley region. The Georgia Tech Research Foundation supported this study.

References

Bailey, R. A. (1989), Geologic map of Long Valley Caldera, Mono-Inyo craters volcanic chain, and vicinity, eastern California, *U.S. Geol. Surv. Misc. Invest. Map*, *I-1933*, scale 1:62,500, pamphlet.

Bailey, R. A., G. B. Dalrymple, and M. A. Lanphere (1976), Volcanism, structure, and geochronology of Long Valley Caldera, Mono County, California, *J. Geophys. Res.*, *81*(5), 725–744, doi:10.1029/JB081i005p00725.

Battaglia, M., C. Roberts, and P. Segall (1999), Magma intrusion beneath Long Valley Caldera confirmed by temporal changes in gravity, *Science*, *285*, 2119–2122, doi:10.1126/science.285.5436.2119.

Battaglia, M., P. Segall, J. Murray, P. Cervelli, and J. Langbein (2003a), The mechanics of unrest at Long Valley Caldera, California: 1. Modeling the geometry of the source using GPS, leveling and two-color EDM data, *J. Volcanol. Geotherm. Res.*, *127*, 195–217, doi:10.1016/S0377-0273(03)00170-7.

Battaglia, M., P. Segall, and C. Roberts (2003b), The mechanics of unrest at Long Valley Caldera, California: 2. Constraining the nature of the source using geodetic and micro-gravity data, *J. Volcanol. Geotherm. Res.*, *127*, 219–245, doi:10.1016/S0377-0273(03)00171-9.

Bos, M. S., R. M. S. Fernandes, S. D. P. Williams, and L. Bastos (2008), Fast error analysis of continuous GPS observations, *J. Geod.*, *82*, 157–166, doi:10.1007/s00190-007-0165-x.

Bursik, M., and K. Sieh (1989), Range front faulting and volcanism in the Mono Basin, eastern California, *J. Geophys. Res.*, *94*(B11), 15,587–15,609, doi:10.1029/JB094iB11p15587.

Castle, R. O., J. E. Estrem, and J. C. Savage (1984), Uplift across Long Valley Caldera, California, *J. Geophys. Res.*, *89*(B13), 11,507–11,516, doi:10.1029/JB089iB13p11507.

Dawson, P. B., J. R. Evans, and H. M. Iyer (1990), Teleseismic tomography of the compressional wave velocity structure beneath the Long Valley region, California, *J. Geophys. Res.*, *95*(B7), 11,021–11,050, doi:10.1029/JB095iB07p11021.

Denlinger, R. P., and F. Riley (1984), Deformation of Long Valley Caldera, Mono County, California, from 1975 to 1982, *J. Geophys. Res.*, *89*(B10), 8303–8314, doi:10.1029/JB089iB10p08303.

Dixon, T. H., A. Mao, M. Bursik, M. Heflin, J. Langbein, R. Stein, and F. Webb (1997), Continuous monitoring of surface deformation at Long Valley Caldera, California, with GPS, *J. Geophys. Res.*, *102*(B6), 12,017–12,034, doi:10.1029/96JB03902.

Dixon, T. H., M. Miller, F. Farina, H. Wang, and D. Johnson (2000), Present-day motion of the Sierra Nevada block and some tectonic implications for the Basin and Range province, North American Cordillera, *Tectonics*, *19*(1), 1–24, doi:10.1029/1998TC001088.

Fialko, Y., M. Simons, and Y. Khazan (2001), Finite source modeling of magmatic unrest in Socorro, New Mexico, and Long Valley, California, *Geophys. J. Int.*, *146*, 191–200, doi:10.1046/j.1365-246X.2001.00453.x.

Fink, J. H. (1985), The geometry of silicic dikes beneath the Inyo Domes, *J. Geophys. Res.*, *90*(B13), 11,127–11,133, doi:10.1029/JB090iB13p11127.

Foulger, G. R., B. R. Julian, A. M. Pitt, D. P. Hill, P. E. Malin, and E. Shalev (2003), Three-dimensional crustal structure of Long Valley Caldera, California, and evidence for the migration of CO_2 under Mammoth Mountain, *J. Geophys. Res.*, *108*(B3), 2147, doi:10.1029/2000JB000041.

Hammond, W. C., and W. Thatcher (2007), Crustal deformation across the Sierra Nevada, northern Walker Lane, Basin and Range transition,

western United States measured with GPS, 2000–2004, *J. Geophys. Res.*, *112*, B05411, doi:10.1029/2006JB004625.

Hildreth, W. (2004), Volcanological perspectives on Long Valley, Mammoth Mountain, and Mono Craters: Several contiguous but discrete systems, *J. Volcanol. Geotherm. Res.*, *136*, 169–198, doi:10.1016/j.jvolgeores.2004.05.019.

Hill, D. P. (1976), Structure of Long Valley Caldera, California, from a seismic refraction experiment, *J. Geophys. Res.*, *81*(5), 745–753, doi:10.1029/JB081i005p00745.

Hill, D. P. (2006), Unrest in Long Valley Caldera, California, 1978–2004, in *Mechanisms of Activity and Unrest at Large Calderas*, edited by C. Troise, G. De Natale, and C. R. J. Kilburn, *Geol. Soc. Spec. Publ.*, vol. 269, pp. 1–24.

Hill, D. P., E. Kissling, J. H. Luetgert, and U. Kradolfer (1985), Constraints on the upper crustal structure of the Long Valley–Mono Craters volcanic complex, eastern California, from seismic refraction measurements, *J. Geophys. Res.*, *90*(B13), 11,135–11,150, doi:10.1029/JB090iB13p11135.

Hill, D. P., J. O. Langbein, and S. Prejean (2003), Relations between seismicity and deformation during unrest in Long Valley Caldera, California, from 1995 through 1999, *J. Volcanol. Geotherm. Res.*, *127*, 175–193, doi:10.1016/S0377-0273(03)00169-0.

Howle, J. F., J. Langbein, C. D. Farrar, and S. K. Wilkinson (2003), Deformation near the Casa Diablo geothermal well field and related processes Long Valley Caldera, eastern California, 1993–2000, *J. Volcanol. Geotherm. Res.*, *127*, 365–390, doi:10.1016/S0377-0273(03)00177-X.

Kelleher, P. C., and K. L. Cameron (1990), The geochemistry of the Mono Craters–Mono lake islands volcanic complex, eastern California, *J. Geophys. Res.*, *95*(B11), 17,643–17,659, doi:10.1029/JB095iB11p17643.

Kleinbaum, D. G., and L. L. Kupper (1978), *Applied Regression Analysis and Other Multivariable Methods*, Duxbury, North Scituate, Mass.

Langbein, J. (1989), Deformation of the Long Valley Caldera, eastern California from mid-1983 to mid-1988: Measurements using a two-color geodimeter, *J. Geophys. Res.*, *94*(B4), 3833–3849, doi:10.1029/JB094iB04p03833.

Langbein, J. (2003), Deformation of the Long Valley Caldera, California: Inferences from measurements from 1988 to 2001, *J. Volcanol. Geotherm. Res.*, *127*, 247–267, doi:10.1016/S0377-0273(03)00172-0.

Langbein, J. (2004), Noise in two-color electronic distance meter measurements revisited, *J. Geophys. Res.*, *109*, B04406, doi:10.1029/2003JB002819.

Langbein, J. (2008), Noise in GPS displacement measurements from southern California and southern Nevada, *J. Geophys. Res.*, *113*, B05405, doi:10.1029/2007JB005247.

Langbein, J., and H. Johnson (1997), Correlated errors in geodetic time series: Implications for time-dependent deformation, *J. Geophys. Res.*, *102*(B1), 591–603, doi:10.1029/96JB02945.

Langbein, J., D. P. Hill, T. N. Parker, and S. K. Wilkinson (1993), An episode of reinflation of the Long Valley Caldera, eastern California: 1989–1991, *J. Geophys. Res.*, *98*(B9), 15,851–15,870, doi:10.1029/93JB00558.

Langbein, J., D. Dzurisin, G. Marshall, R. Stein, and J. Rundle (1995), Shallow and peripheral volcanic sources of inflation revealed by modeling two-color geodimeter and leveling data from Long Valley Caldera, California, 1988–1992, *J. Geophys. Res.*, *100*(B7), 12,487–12,495, doi:10.1029/95JB01052.

Mao, A., C. G. A. Harrison, and T. H. Dixon (1999), Noise in GPS coordinate time series, *J. Geophys. Res.*, *104*(B2), 2797–2816, doi:10.1029/1998JB900033.

Marshall, G. A., J. Langbein, R. S. Stein, M. Lisowski, and J. Svarc (1997), Inflation of Long Valley Caldera, California, Basin and Range strain, and possible Mono Craters dike opening from 1990–94 GPS surveys, *Geophys. Res. Lett.*, *24*(9), 1003–1006, doi:10.1029/97GL00885.

McTigue, D. F. (1987), Elastic stress and deformation near a finite spherical magma body: Resolution of the point source paradox, *J. Geophys. Res.*, *92*(B12), 12,931–12,940, doi:10.1029/JB092iB12p12931.

Mogi, K. (1958), Relations between the eruption of various volcanoes and the deformation of the ground surface around them, *Bull. Earthquake Res. Inst. Univ. Tokyo*, *36*, 99–134.

Newman, A. V., T. H. Dixon, G. I. Ofoegbu, and J. E. Dixon (2001), Geodetic and seismic constrains on recent activity at Long Valley Caldera, California: Evidence for viscoelastic rheology, *J. Volcanol. Geotherm. Res.*, *105*, 183–206, doi:10.1016/S0377-0273(00)00255-9.

Newman, A. V., T. H. Dixon, and N. Gourmelen (2006), A four-dimensional viscoelastic deformation model for Long Valley Caldera, California, between 1995 and 2000, *J. Volcanol. Geotherm. Res.*, *150*, 244–269, doi:10.1016/j.jvolgeores.2005.07.017.

Prejean, S., W. Ellsworth, M. Zoback, and F. Waldhauser (2002), Fault structure and kinematics of the Long Valley Caldera region, California, revealed by high-accuracy earthquake hypocenters and focal mechanism stress inversions, *J. Geophys. Res.*, *107*(B12), 2355, doi:10.1029/2001JB001168.

Press, W. H., S. A. Teukolsky, W. T. Vetterling, and B. P. Flannery (1992), *Numerical Recipes in FORTRAN: The Art of Scientific Computing*, 2nd ed., Cambridge Univ. Press, New York.

Ryall, A., and F. Ryall (1983), Spasmodic tremor and possible magma injection in Long Valley Caldera, eastern California, *Science*, *219*, 1432–1433, doi:10.1126/science.219.4591.1432.

Sanders, C. O., S. C. Ponko, L. D. Nixon, and E. A. Schwartz (1995), Seismological evidence for magmatic and hydrothermal structure in Long Valley Caldera from local earthquake attenuation and velocity tomography, *J. Geophys. Res.*, *100*(B5), 8311–8326, doi:10.1029/95JB00152.

Savage, J. C., and M. M. Clark (1982), Magmatic resurgence in Long Valley Caldera, California: Possible cause of the 1980 Mammoth lakes earthquakes, *Science*, *217*, 531–533, doi:10.1126/science.217.4559.531.

Savage, J. C., and R. S. Cockerham (1984), Earthquake swarm in Long Valley Caldera, California, January 1983: Evidence for dike inflation, *J. Geophys. Res.*, *89*(B10), 8315–8324, doi:10.1029/JB089iB10p08315.

Savage, J. C., M. Lisowski, W. H. Prescott, and N. E. King (1981), Strain accumulation near the epicenter of the 1978 Bishop and 1980 Mammoth Lakes, California, earthquakes, *Bull. Seismol. Soc. Am.*, *71*, 465–476.

Sorey, M. L., C. D. Farrar, G. A. Marshall, and J. F. Howle (1995), Effects of geothermal development on deformation in the Long Valley Caldera, eastern California, 1985–1994, *J. Geophys. Res.*, *100*(B7), 12,475–12,486, doi:10.1029/95JB00955.

Steck, L. K. (1995), Simulated annealing inversion of teleseismic P-wave slowness and azimuth for crustal velocity structure at Long Valley Caldera, *Geophys. Res. Lett.*, *22*(4), 497–500, doi:10.1029/94GL03050.

Suemnicht, G. A., and R. J. Varga (1988), Basement structure and implications for hydrothermal circulation patterns in the western moat of Long Valley Caldera, California, *J. Geophys. Res.*, *93*(B11), 13,191–13,207, doi:10.1029/JB093iB11p13191.

Tiampo, K. F., J. B. Rundle, J. Fernandez, and J. O. Langbein (2000), Spherical and ellipsoidal volcanic sources at Long Valley Caldera, California, using a generic algorithm inversion technique, *J. Volcanol. Geotherm. Res.*, *102*, 189–206, doi:10.1016/S0377-0273(00)00185-2.

Tizzani, P., P. Berardino, F. Casu, P. Euillades, M. Manzo, G. P. Ricciardi, G. Zeni, and R. Lanari (2007), Surface deformation of Long Valley Caldera and Mono Basin, California, investigated with the SBAS-InSAR approach, *Remote Sens. Environ.*, *108*, 277–289, doi:10.1016/j.rse.2006.11.015.

Turcotte, D. L., and G. Schubert (2002), *Geodynamics*, 2nd ed., Cambridge Univ. Press, New York.

Waldhauser, F., and D. P. Schaff (2008), Large-scale relocation of two decades of northern California seismicity using cross-correlation and double-difference methods, *J. Geophys. Res.*, *113*, B08311, doi:10.1029/2007JB005479.

Wdowinski, S., Y. Bock, J. Zhang, P. Fang, and J. Genrich (1997), Southern California Permanent GPS Geodetic Array: Spatial filtering of daily positions for estimating coseismic and postseismic displacements induced by the 1992 Landers earthquakes, *J. Geophys. Res.*, *102*(B8), 18,057–18,070, doi:10.1029/97JB01378.

Webb, F. H., M. Bursik, T. Dixon, F. Farina, G. Marshall, and R. S. Stein (1995), Inflation of Long Valley Caldera from one year of continuous GPS observations, *Geophys. Res. Lett.*, *22*(3), 195–198, doi:10.1029/94GL02968.

Weiland, C. M., L. K. Steck, P. B. Dawson, and V. A. Korneev (1995), Nonlinear teleseismic tomography at Long Valley Caldera, using three-dimensional minimum travel time ray tracing, *J. Geophys. Res.*, *100*(B10), 20,379–20,390, doi:10.1029/95JB01147.

Wessel, P., and W. H. F. Smith (1991), Free software helps map and display data, *Eos Trans. AGU*, *72*, 441.

Williams, S. D. P. (2003), The effect of coloured noise on the uncertainties of rates estimated from geodetic time series, *J. Geod.*, *76*, 483–494, doi:10.1007/s00190-002-0283-4.

Yang, X., P. M. Davis, and J. H. Dieterich (1988), Deformation from inflation of a dipping finite prolate spheroid in an elastic half-space as a model for volcanic stressing, *J. Geophys. Res.*, *93*(B5), 4249–4257, doi:10.1029/JB093iB05p04249.

Zhang, J., Y. Bock, H. Johnson, P. Fang, S. Williams, J. Genrich, S. Wdowinski, and J. Behr (1997), Southern California permanent GPS geodetic array: Error analysis of daily position estimates and site velocities, *J. Geophys. Res.*, *102*(B8), 18,035–18,055, doi:10.1029/97JB01380.

L. Feng and A. V. Newman, School of Earth and Atmospheric Sciences, Georgia Institute of Technology, 311 Ferst Drive, ES&T Room 2254, Atlanta, GA 30332-0340, USA. (lfeng@gatech.edu; anewman@gatech.edu)